

EXCITED STATES IN ^{52}Fe AND THE ORIGIN OF THE YRAST TRAP AT $I^\pi=12^+$

C.A. Ur^{1,2}, D. Bucurescu², S.M. Lenzi¹, G. Martínez-Pinedo³, D.R. Napoli⁴,
D. Bazzacco¹, F. Brandolini¹, D.M. Brink⁵, J.A. Cameron⁶, G.de Angelis⁴, M. De Poli⁴,
A. Gadea⁴, S. Lunardi¹, N. Mărginean², M.A. Nagarajan⁷, P. Pavan¹,
C. Rossi Alvarez¹, C.E. Svensson⁶

¹*Dipartimento di Fisica and INFN, Sezione di Padova, Padova, Italy*

²*H.Hulubei National Institute of Physics and Nuclear Engineering, Bucharest, Romania*

³*W.K. Kellogg Radiation Laboratory, California Institute of Technology, Pasadena, USA*

⁴*Laboratori Nazionali di Legnaro, INFN, Legnaro, Italy*

⁵*Dipartimento di Fisica and INFN, Trento, Italy*

⁶*McMaster University, Ontario, Canada*

⁷*Department of Physics, UMIST, Manchester, United Kingdom*

(May 28, 2022)

Excited states in ^{52}Fe have been determined up to spin $10\hbar$ in the reaction $^{28}\text{Si} + ^{28}\text{Si}$ at 115 MeV by using γ -ray spectroscopy methods at the GASP array. The excitation energy of the yrast 10^+ state has been determined to be 7.381 MeV, almost 0.5 MeV above the well known β^+ -decaying yrast 12^+ state, definitely confirming the nature of its isomeric character. The mean lifetimes of the states have been measured by using the Doppler Shift Attenuation method. The experimental data are compared with spherical shell model calculations in the full pf -shell.

KEYWORDS: ^{52}Fe excited states, gamma-ray spectroscopy, angular distributions, DSAM lifetime measurement, yrast trap, spherical shell model.

PACS: 21.10.-k, 21.10.Tg, 21.60.Cs, 23.20.Lv, 27.40.+z

I. INTRODUCTION

Recently, the study of the $f_{7/2}$ -shell nuclei has gained renewed interest. The development of very efficient detector arrays both for γ -rays and charged particles has allowed investigation of the structure of these nuclei at high spins. Close to the middle of the $f_{7/2}$ shell, nuclei show strong collective behaviour near the ground state [1–3]. At higher spins, shape transitions towards triaxial and non-collective deformations can occur due to an intimate interplay between the collective and microscopic degrees of freedom. Recently, band terminating states, corresponding to fully aligned $f_{7/2}$ configurations, were observed in ^{48}Cr [2] and ^{50}Cr [3]. When approaching the doubly magic nucleus ^{56}Ni the collective behaviour is rapidly disappearing as nuclei evolve towards a spherical shape. So far, the nucleus ^{52}Fe has been an experimental challenge. Most of the known excited states in this nucleus are of relatively low spin (below $6\hbar$) and have been observed in ($^3\text{He},n$) [4–6], ($\alpha,2n$) [7] and (p,t) [8] reactions (see also ref. [9]). Attempts to extend its yrast structure to higher spins in fusion-evaporation reactions induced by heavy ions have failed so far (see refs. [10,11] and references therein). The reason of this has been attributed to the probable inversion between the lowest 10^+ and 12^+ states, which results in an isomeric 12^+ yrast trap that decays by β^+ emission to ^{52}Mn [11,12]. Thus, although fusion-evaporation reactions populate appreciably the ^{52}Fe channel, the deexcitation γ -ray flux

effectively stops at the 12^+ level where it is diverted into the population of high spin states in ^{52}Mn . Due to the weak direct population of the lower spin states, it was not possible to observe the yrast line above the 4_1^+ state [11]. One should note, however, that these previous experiments were performed with small (10-15% efficiency) Ge(Li) detectors, and therefore had a rather low γ -ray detection efficiency.

In this work, performed with a powerful γ -ray detector array, we have been able to extend the level scheme of ^{52}Fe up to the 10^+ state, thereby confirming the predicted inversion of the 10^+ and 12^+ states.

The experimental data have been interpreted in the framework of spherical shell model (SM) calculations in the full pf shell.

II. EXPERIMENTAL DETAILS

High spin states in the nucleus ^{52}Fe have been populated via the $^{28}\text{Si} + ^{28}\text{Si}$ reaction at 115 MeV beam energy. The silicon beam was delivered by the XTU Tandem accelerator at the National Laboratory of Legnaro. The target was a 0.8 mg/cm^2 ^{28}Si foil evaporated on a 13 mg/cm^2 Au backing. Gamma rays have been detected with the GASP array [13] which consists of 40 Compton-suppressed large volume HP Ge detectors and the 80 BGO crystals inner ball. The 40 Ge detectors are placed symmetrically relative to the beam axis on seven

rings as follows: 6 detectors at 35°, 6 detectors at 60°, 4 detectors at 72°, 8 detectors at 90°, 4 detectors at 108°, 6 detectors at 120° and 6 detectors at 145°. Data have been recorded when at least two Ge detectors and two elements of the BGO inner ball fired in coincidence. We collected on tape a total of 7.8×10^8 two fold and 5.4×10^7 three fold events. Gain matching and efficiency calibration of the Ge detectors have been performed using ^{152}Eu and ^{56}Co radioactive sources. The total cross section of the reaction used was fragmented in a large number of reaction channels. In order to estimate the relative yield of these channels we have used a total γ - γ coincidence matrix in which we determined the intensities of the γ -ray transitions feeding the ground states. The most intense channels populated in our reaction were ^{50}Cr ($\alpha 2p$) with $\sim 31\%$, ^{49}Cr ($\alpha 2pn$) with $\sim 29\%$ and ^{49}V ($\alpha 3p$) with $\sim 11\%$ of the total cross section. States in ^{52}Fe have been populated either by $2p2n$ or α evaporation. The population of the ground state of ^{52}Fe was estimated to represent less than 1% of the total gamma yield.

III. DATA ANALYSIS

A. The level scheme

Previous studies of ^{52}Fe [6,8,11,14] have established the position of the yrast 2^+ , 4^+ , 3^- and 5^- states, of a second 4^+ state and of the long lived 12^+ state. This isomeric level, placed at an excitation energy of 6820 ± 130 keV and with a measured half-life of 45.94 ± 1.0 sec [11], decays β^+ towards states in ^{52}Mn . An upper limit of 0.4 % was established [11] for the γ -decay of the 12^+ state. The high efficiency of the GASP array and the use of a reaction in which low-lying levels are considerably populated by side feeding allowed us to identify new γ -ray transitions belonging to ^{52}Fe by setting gates on the previously known γ -rays. Double gated γ -coincidence spectra with gates set on some key transitions assigned to ^{52}Fe are shown in Fig. 1. On the basis of such γ - γ coincidence data obtained from a γ - γ - γ coincidence cube and of the relative intensities of the transitions, we have constructed the level scheme shown in Fig. 2. The relative intensities of the transitions have been extracted from the 90° spectrum in coincidence with the 850 keV $2^+ \rightarrow 0^+$ transition in order to avoid the uncertainties introduced by the lineshape broadening. The intensity for the 2753 keV transition which is assumed to be of $\Delta I=1$ character (see level scheme) is already corrected for the angular distribution as specified in ref. [15]. The high energy part of the spectrum at 90° in coincidence with the 850 keV transition, from which the relative intensities were extracted, is shown in Fig. 3.

We could confirm the yrast 6^+ state suggested in ref. [6]; furthermore we established a new 6^+ state as well as two 8^+ states and a 10^+ state lying at 7.381 MeV, well

above the 12^+ β^+ decaying isomer. This constitutes the first experimental evidence for the predicted [11] inversion between the first 10^+ and 12^+ states. Three new γ -rays connecting the 5^- level to the 3^- , 4_1^+ and 4_2^+ states have been identified. We have to mention here that high spin states in ^{52}Fe have been also identified in a parallel experiment performed recently at Gammasphere [16].

The low statistics together with the high background produced by the more strongly populated nuclei in this reaction, prevented the observation of a possible E4 γ -ray connecting the 12^+ and the 8^+ states.

Spins and parities have been assigned on the basis of the angular distribution of the γ -rays. Data were sorted in two γ - γ coincidence matrices having on one axis γ -rays detected at all angles and on the second axis those detected at 60° and 120° and those detected at 90° , respectively. By setting gates on the axis with all the detectors, the intensity of the observed γ -rays follows the regular angular distribution law disregarding the multipole character of the gating transition. The ADO (Angular Distribution from Oriented states) ratio is defined as [17]:

$$R_{ADO} = \frac{(I_\gamma(\theta) + I_\gamma(\pi - \theta))/2}{I_\gamma(90^\circ)}$$

where I_γ denotes the intensity of the observed γ -ray at the angles θ , $\pi - \theta$ and 90° , respectively, corrected by the detection efficiency. Typical values of the ADO ratios for $\theta=60^\circ$ in the GASP geometry are ~ 1.17 for a stretched quadrupole transition and ~ 0.85 for a stretched dipole transition. The γ -ray energies and relative intensities of the transitions belonging to ^{52}Fe , together with their ADO ratios at 60° and spin-parity assignments are reported in Table I. Spin and parity of the new levels are based on ADO analysis, by assuming that transitions with $R_{ADO} \approx 1.17$ have stretched E2 character. The results for the 1941, 2168 and 889 keV transitions lead therefore to $I^\pi = 10^+$ for the state at 7.381 MeV.

We could not extract the angular distribution of the 2735 keV and 2753 keV γ -ray transitions depopulating the 4_2^+ and 5^- states, respectively, since their broadened lineshapes are overlapping. The spin assignment for the states decaying via these two transitions are based on previous measurements. In ref. [6] the angular distribution of the 2735 keV transition was found to be compatible with an E2 character. This assignment is now supported by the observation of a 1286 keV transition connecting the 6_2^+ state to the 4_2^+ state. A level at 5138 ± 4 keV excitation energy decaying towards the 4^+ yrast state was also reported in ref. [6]; later on [8], a 5^- assignment has been given to that state. This brings a $\Delta I=1$ character for the new measured γ -ray transitions of 1553 keV and 2753 keV. The 5^- assignment is also confirmed by the E2 character of the 740 keV γ -ray feeding the 3^- state.

B. DSAM analysis

To perform the analysis of the Doppler broadened lineshapes we sorted the data in seven 4k x 4k γ - γ coincidence matrices, each corresponding to the coincidence between the detectors of one ring and all other detectors.

We have analyzed the γ -ray spectra in coincidence with the 850 keV γ -ray (which does not show any appreciable broadening) in order to select better the channel of interest and to reduce as much as possible the contaminations on the lineshapes of the relevant transitions.

The $10^+ \rightarrow 8_1^+$ and $10^+ \rightarrow 8_2^+$ γ -ray transitions do not exhibit a broadened lineshape, indicating that the 10^+ state has a long lifetime (longer than a few ps). Changes in the lineshape for states below were observed only when a large amount of side feeding was present (see Table I).

The lifetime analysis was carried out with the computer code LINESHAPE [18]. The slowing down process and the scattering of the recoils in the target and in the backing were described by a Monte Carlo simulation as it was developed by Bacelar *et al.* [19], with a modification regarding the spread in the initial direction of the recoils due to the evaporation of light particles [20]. The simulation was performed with 5000 histories and up to 187 time steps covering the recoil range in the backing. Northcliffe and Schilling [21] electronic stopping power values have been used in the calculations.

The program performs a χ^2 minimization of the lineshape fit as a function of the level lifetime, the side-feeding time and the normalization factors. We have used a one step side-feeding for each level, the side-feeding intensity being a fix parameter in the program. The background and the intensity of contaminant peaks present in the spectra have been kept fixed. The analysis was done for each line separately starting with the highest transition in the level scheme. Lineshapes were fitted at forward and backward angles simultaneously allowing a better identification of the contaminants. The program, designed to deal with cascades of γ -rays connecting states with side-feeding originating only from the continuum, is not suited for level schemes such as that of ^{52}Fe . Anyway, it could be used also in our case by properly transforming the complex feeding scheme in equivalent γ -ray cascades. We have first determined the lifetimes of the two 8^+ states from the analysis of the two decay branches, $10^+ \rightarrow 8_1^+ \rightarrow 6_1^+$ and $10^+ \rightarrow 8_2^+ \rightarrow 6_1^+$, respectively. The lifetime of the yrast 6^+ state has been extracted by analyzing the decay pattern along the yrast sequence. To account for the feeding provided via the decay of the 8_2^+ state, we have introduced above the 6_1^+ state a virtual level with zero lifetime and side-feeding time given by the lifetime of the 8_2^+ state. The intensity of the 1021 keV transition has been modified to account for the whole longlived population of the 6_1^+ level provided by the decay of the 10^+ state. The lifetime of the second 6^+ state has been extracted from the analysis of the sequence of

γ -ray transitions $10^+ \rightarrow 8_2^+ \rightarrow 6_2^+ \rightarrow 4_1^+$. In order to describe the multiple feeding of the 4_1^+ state, we have again introduced virtual levels of mean lifetime equal to zero and side-feeding times given by the lifetimes of the 6_2^+ and 5^- states, respectively. In Fig. 4 the best fits for the lineshapes (measured at 72°) of several γ -ray transitions are displayed. The lineshape of the 2035 keV transition is strongly contaminated by the presence of the 2045 keV line belonging to ^{49}Cr with a very pronounced lineshape. We have determined the lifetime of the 8_1^+ state from the best fit of the experimental spectrum with that obtained after summing the calculated lineshape of the 2035 keV γ -ray transition and the experimental lineshape of the contaminant line. The two lines of 2735 and 2753 keV overlapped their lineshapes and consequently, we could not extract a definite lifetime value for the 4_2^+ and 5^- states. We estimated a lower limit of about 1 ps for the sidefeeding of the 4_1^+ provided via the 2753 keV transition. We have varied this sidefeeding time in the range 0.5–2.0 ps without practically affecting the mean lifetime value of the 4_1^+ state. The obtained results are reported in Table II together with the previous measured values. The experimental reduced transition probabilities $B(E2)$ have been extracted according to the expression [22]:

$$B(E2) (e^2b^2) = \frac{0.08156 B_\gamma}{\tau E_\gamma^5 (1 + \alpha_{tot})}$$

where B_γ is the branching ratio of the γ -ray transition, τ is the lifetime of the state in picoseconds, E_γ is the energy of the transition in MeV and α_{tot} is the total conversion coefficient. These $B(E2)$ values are compared to the ones calculated within the SM (see Sect. IV.A).

IV. DISCUSSION

A. Shell Model Calculations

The structure of ^{52}Fe has been analyzed in the framework of the spherical shell model in the full pf shell (m -scheme dimension 109,954,620). These calculations have shown to reproduce with very good accuracy the experimental data of the nuclei in this mass region [2,3,23–25]. The single particle energies were taken from the ^{41}Ca experimental spectrum and the effective interaction used was the KB3 [26]. The effects of core polarization on the quadrupole properties were taken into account by using the effective charges $q_\pi=1.5$ and $q_\nu=0.5$. The hamiltonian was treated by the Lanczos method and diagonalized with the code ANTOINE [27]. The resulting theoretical level scheme is compared in Fig. 5 with the experimental one. A fairly good agreement is found. The energy inversion of the 12^+ isomeric state with the 10^+ yrast is reproduced theoretically, even if the energy gap between the two states is smaller than in the experiment.

A reasonable reproduction of the energy spectrum is not enough to establish the goodness of the shell model

calculations. A more stringent test is their ability to reproduce the experimental lifetimes or the $B(E2)$ values. The calculated $B(E2)$ values are displayed in Table II. They are in good agreement with the experimental ones. The values for the 6_2^+ and the 8_2^+ states seem to be not very well described by the calculations but this can be due to the vicinity in energy to the states of the same spin and parity (see Fig. 2).

The shell model calculations provide also the spectroscopic quadrupole moments Q_{spec} which are plotted in the lowest panel of Fig. 6. Large negative values are obtained for the first two excited states. As already pointed out in ref. [28], ^{52}Fe behaves as a rotor below $I = 6\hbar$, consistently with a $K = 0$ band. Using the rotational model prescription we obtained for the 2^+ and 4^+ states an intrinsic quadrupole moment $Q_0 \approx 90 \text{ e fm}^2$ from both the theoretical $B(E2)$ values and the spectroscopic quadrupole moments. The deduced deformation parameter is $\beta = 0.23$. At $I = 6\hbar$, Q_{spec} changes sign and takes a very small value. This change of regime can be associated to the process of particle alignment. In this mass region, the most deformed nuclei lay in the middle of the shell. In particular, the nucleus ^{48}Cr has the maximum number of particles to develop quadrupole collectivity. At high spin, the interplay between single particle and collective degrees of freedom produces changes of shape towards spherical or non collective oblate states. This is consistent with the fact that the mechanism of generating angular momentum by aligning the valence particle spins along the rotational axis in a high- j shell becomes energetically favoured at high frequency. Nuclei as ^{52}Fe which do not lay near the middle of the shell, are not much deformed and the incipient rotational behaviour at low spin smears out very soon with increasing angular momentum.

Recently, it has been shown that the development of quadrupole coherence that gives rise to rotational-like bands in these nuclei [29], is originated by the mixing of the $f_{7/2}$ and $p_{3/2}$ orbits. It is thus interesting to follow the single orbital contributions to the wavefunction as the angular momentum increases. In Fig. 6, the fractional occupation numbers of the $f_{7/2}$ and $p_{3/2}$ orbits are plotted for the yrast states of ^{52}Fe . For comparison, the same quantities are also reported for its cross conjugate nucleus ^{44}Ti and for the most quadrupole deformed nucleus in the $f_{7/2}$ shell, ^{48}Cr . In the simple $(f_{7/2})^n$ model, ^{52}Fe and ^{44}Ti should have the same energy spectra (cross conjugate symmetry). In fact, the two level schemes are similar at low spin. However, the symmetry is lost at high spin: there is no inversion of the 10^+ and 12^+ states in ^{44}Ti . Then, even if from a qualitative analysis of Fig. 6 the $f_{7/2}$ subshell results by large the most occupied one, the contribution arising from the rest of the orbitals in the pf shell becomes crucial to obtain a good description of these nuclei. The fractional occupation number of the $p_{3/2}$ orbital is much more important than the other two orbitals $f_{5/2}$ and $p_{1/2}$ (not included in the figure). At low

spin, the $p_{3/2}$ occupation number remains almost constant for all three nuclei. The biggest $p_{3/2}$ contribution is observed for the most deformed nucleus ^{48}Cr , where it begins to decrease at the backbending ($I = 10\hbar$). In ^{52}Fe this happens much earlier, at $I = 6\hbar$.

At the maximum spin that can be constructed with the valence particles in the $f_{7/2}$ shell, the $p_{3/2}$ occupation number vanishes for ^{44}Ti ($I = 12\hbar$) and becomes insignificant for ^{48}Cr ($I = 16\hbar$). Also the smaller contribution from the $f_{5/2}$ and $p_{1/2}$ decreases at high spin and at the band terminating states the $f_{7/2}$ becomes the only relevant orbit. These fully-aligned band-terminating states are of non collective character. The situation is different in ^{52}Fe , where above $I = 6\hbar$, the $p_{3/2}$ -shell contribution stays almost constant as a function of spin and the same happens for the other components, even at $I = 12\hbar$. There is still some quadrupole coherence in the 12^+ state. This can be related to the energy inversion of the 10^+ and 12^+ states, which gives rise to the yrast trap, as will be shown below.

The change of regime at $I = 6\hbar$, reflected in the fractional occupation numbers and in the spectroscopic quadrupole moments, can be related in the rotational model to a crossing between the ground state $K = 0$ band and an excited $K = 6$ band. To study this problem we have computed different Nilsson intrinsic states and projected them onto good angular momentum. The $K = 0$ band corresponds to an intrinsic state obtained by filling the $[330]1/2$, $[321]3/2$, $[312]5/2$ Nilsson orbitals for protons and neutrons. The intrinsic state of the $K = 6$ band is constructed by exciting one proton *or* one neutron from the $[312]5/2$ to the $[303]7/2$ orbital. Our calculations indicate that the $I = 6$ $K = 6$ and the $I = 6$ $K = 0$ are degenerate. This also explains the presence of two 6^+ levels close in energy (see Fig. 2). The states between the 6^+ and the 10^+ could be thus considered as a mixing of a $K = 0$ and a $K = 6$ band. We cannot speak of a well defined intrinsic state.

We repeated this procedure for the state at $I = 12\hbar$, where there is a residual quadrupole coherence. A $K = 12$ intrinsic prolate Nilsson state can be constructed by exciting two particles, a proton *and* a neutron, from the $[312]5/2$ to the $[303]7/2$ orbit. After projecting this state onto good angular momentum, an overlap of ~ 0.9 with the exact shell model wave function of the 12^+ state is obtained. The excitation energy of this level is lower than the $I = 10\hbar$ and $I = 12\hbar$ states coming from the $K = 0$ and $K = 6$ bands, which explains the presence of the yrast trap.

B. The systematics of yrast traps

Excited nuclear states in the vicinity of closed shells are explained through the rearrangement of the nucleons in the available single particle orbitals. This results usually in irregular decay patterns and isomeric states,

often called, at high spins, “yrast traps”. The isomeric 12^+ state in ^{52}Fe represents an energy spin yrast trap due to the large difference of its spin with those of the lower states.

Several high spin yrast traps have been identified along the periodic table but only few of them originate through the inversion in energy with yrast states of lower spins. Such yrast traps have been identified in ^{53}Fe [12], ^{53}Co [30], ^{156}Hf [31], ^{211}Po [32] and ^{212}Po [33]. The nature of the energy spin traps can be related [34] to the alignment of nucleons. The nucleons with aligned spins gain energy because their residual interaction is stronger for wave functions with large spatial overlap (MONA effect [35]). In most of the cases the structure of these states is associated with oblate deformation or “single particle” rotations. A different structure is, however, found in ^{52}Fe where the effect of the maximum alignment is accompanied by a quadrupole coherence that gives rise to a prolate deformation at $I = 12\hbar$, as stated in the previous subsection.

In Fig. 7a, the yrast bands of the even-even $N=Z$ nuclei ^{44}Ti , ^{48}Cr and ^{52}Fe are shown up to the maximum spin that can be built in the $f_{7/2}$ shell. The nucleus ^{48}Cr , is presented to stress the evolution of the collectivity along the $N=Z$ line. The similarity between the level structure for ^{44}Ti and ^{52}Fe can be seen up to spin $10\hbar$ but in ^{44}Ti , even if the energy of the 12^+ state is lowered due to the alignment of the valence nucleons, no inversion is observed. As discussed in the previous subsection, in ^{44}Ti and ^{48}Cr the $I = 12\hbar$ and $I = 16\hbar$ levels, respectively, behave as non collective band terminating states with pure $f_{7/2}$ configurations. On the other hand, the 12^+ state in ^{52}Fe still preserves contributions from the $p_{3/2}$ orbital, the nucleus is slightly prolate deformed and therefore more collective.

In Fig. 7b, one can see the systematics of other yrast traps in this mass region. The nucleus ^{53}Fe and its mirror ^{53}Co present yrast traps at $I = 19/2\hbar$ at an excitation energy around 3 MeV that lay below the $15/2^-$ states. The $19/2^-$ level in ^{53}Fe decays by γ emission of E4, M5 and E6 character, while in ^{53}Co decays β^+ . In these cases the yrast traps are also well reproduced by the shell model calculations. In the Nilsson calculation, we obtain a prolate $K = 19/2$ state for ^{53}Fe (^{53}Co) by exciting one of the protons (neutrons) from the $[312]5/2$ to the $[303]7/2$ and coupling them to the odd neutron (proton). As in the case of the $N = Z$ ^{52}Fe , these aligned collective states are favoured in energy and become yrast traps. These mirror nuclei do not behave as their cross conjugates $A = 43$. In fact, in ^{43}Ti and ^{43}Sc there are isomeric $19/2^-$ states at about 3 MeV excitation energy but higher in energy with respect to the $15/2^-$ states to which they decay by γ emission. The systematics shows that the cross conjugate symmetry is not verified in these nuclei. One can interpret these differences in terms of deformation or available valence space. In fact, at the beginning of the shell, ^{44}Ti together with the mirrors

$A = 43$, have a reduced number of particles and the fully aligned states are of pure $(f_{7/2})^n$ configuration of non-collective character. For the heavier group of nuclei, the maximum spin state is slightly prolate deformed due to the contribution of the $p_{3/2}$ orbit and yrast traps can be formed.

V. CONCLUSIONS

We have investigated high spin states in ^{52}Fe in a backed target experiment. The high detection efficiency of the GASP array and the relatively large amount of side-feeding population of the states of interest allowed us to establish the level scheme up to spin $I = 10\hbar$, a fact which was hindered until now by the presence of the 12^+ yrast trap. We could therefore establish experimentally that the retardation of the decay of the 12^+ yrast state is due to its location at an energy lower than that of the 10^+ state. The mean lifetime of the states have been determined by means of the Doppler Shift Attenuation Method.

The experimental results have been compared with calculations performed within the spherical SM in the pf shell. Reasonably good agreement has been found for both the energy of the states and the $B(E2)$ values. The difference between the 12^+ states in the cross conjugate nuclei ^{44}Ti and ^{52}Fe can be satisfactorily explained through shell model calculations. It was concluded that apart from the lowering of the states due the maximal overlapping of the nucleonic wave functions, in ^{52}Fe this state is even lower due to a higher degree of collectivity present in the structure of the wave function related to the contribution of the $p_{3/2}$ orbital.

ACKNOWLEDGMENTS

The authors would like to thank B.F. Bayman, E. Caurier, A. Poves, D. Rudolph and A.P. Zuker for fruitful and interesting discussions. We also thank the crew of the XTU Tandem of the National Laboratory of Legnaro for the smooth operation of the accelerator during the experiment. The computational cycles were provided by the Centro de computación científica de la Facultad de Ciencias at the Universidad Autónoma de Madrid. G.M.P. was partly supported by the DGICYES (Spain) and A.G. was supported by the EC under contract number ER-BCHBGCT940713.

-
- [1] J.A. Cameron, M.A. Bentley, A.M. Bruce, R.A. Cunningham, W. Gelletly, H.G. Price, J. Simpson, D.D. Warner and A.N. James, Phys. Rev. C **49** (1994) 1347.

- [2] S.M. Lenzi, D.R. Napoli, A. Gadea, M.A. Cardona, D. Hojman, M.A. Nagarajan, C. Rossi Alvarez, N.H. Medina, G. de Angelis, D. Bazzacco, M.E. Debray, M. De Poli, S. Lunardi and D. De Acuña, *Z. Phys A* **354** (1996) 117.
- [3] S.M. Lenzi, C.A. Ur, D.R. Napoli, M.A. Nagarajan, D. Bazzacco, D.M. Brink, M.A. Cardona, G. de Angelis, M. De Poli, A. Gadea, D. Hojman, S. Lunardi, N.H. Medina and C. Rossi Alvarez, *Phys. Rev. C* **56** (1997) 1313.
- [4] W.P. Alford, R.A. Lindgren, D. Elmore and R.N. Boyd, *Nucl. Phys.* **A243** (1975) 269.
- [5] W. Bohne, H. Fuchs, K. Grabisch, D. Hilscher, U. Jahnke, H. Kluge, T.G. Masterson and H. Morgenstern, *Nucl. Phys.* **A245** (1975) 107.
- [6] Y. Iritani, J. Kasagi and H. Ohnuma, *J. Phys. Soc. Jap.* **43** (1977) 1119.
- [7] D. Evers, A. Harasim, R.L. McGrath and W. Assmann, *Phys. Rev. C* **15** (1977) 1690.
- [8] P. Decowski, W. Benenson, B.A. Brown and H. Nann, *Nucl. Phys.* **A302** (1978) 186.
- [9] Huo Junde, *Nucl. Data Sheets* **71** (1994) 659.
- [10] V. Avrigeanu, D. Bucurescu, G. Constantinescu, E. Dragulescu, M. Ivascu, D. Pantelica and R. Teodorescu, *Nucl. Phys.* **A272** (1976) 243.
- [11] D.F. Geesaman, R.L. McGrath, J.W. Noe and R.E. Malmin, *Phys. Rev. C* **19** (1979) 1938.
- [12] D.F. Geesaman, R.E. Malmin, R.L. McGrath and J.W. Noe, *Phys. Rev. Lett.* **34** (1975) 326.
- [13] D. Bazzacco, in *Proceedings of the International Conference on Nuclear Structure at High Angular Momentum, Ottawa, 1992* [Report No. AECL 10613], Vol.II, p.376.
- [14] J.B. Viano, Y. Dupont and J. Menet, *Phys. Lett.* **B34** (1971) 397.
- [15] T. Yamazaki, "Tables of Coefficients for Angular Distribution of Gamma Rays from Aligned Nuclei", *Nucl. Data* **3** (1967) 1.
- [16] M. Abdelrazek *et al.*, University of Tennessee Progress Report (1997) 12.
- [17] M. Piiparinen, A. Ataç, J. Blomqvist, G.B. Hagemann, B. Herskind, R. Julin, S. Juutinen, A. Lampinen, J. Nyberg, G. Sletten, P. Tikkanen, S. Tormanen, A. Virtanen and R. Wyss, *Nucl. Phys.* **A605** (1996) 191.
- [18] J.C. Wells and N.R. Johnson. "LINESHAPE: a Computer Program for Doppler-Broadened Lineshape Analysis", Report No. ORNL-6689 (1991), p.44.
- [19] J.C. Bacelar, A. Holm, R.M. Diamond, E.M. Beck, M.A. Deleplanque, J. Draper, B. Herskind and F.S. Stephens, *Phys. Rev. Lett.* **57** (1986) 3019; *Phys. Rev. C* **35** (1987) 1170.
- [20] F. Brandolini, S.M. Lenzi, D.R. Napoli, R.V. Ribas, H. Somacal, C.A. Ur, D. Bazzacco, J.A. Cameron, G.de Angelis, M.De Poli, A. Gadea, C. Fahlander, S. Lunardi, M.A. Nagarajan, C.Rossi Alvarez and C. Svensson, in *Proceedings of the International Symposium on Exotic Nuclear Shapes, Debrecen, May 12-17 1997 (to be published)*.
- [21] L.C. Northcliffe and R.F. Schilling, *Nucl. Data Tables* **7** (1970) 233.
- [22] H.Ejiri and M.J.A.de Voigt, *Gamma Ray and Electron Spectroscopy in Nuclear Physics*, ed. P.E.Hodgson, Clarendon Press - Oxford, Chapt.6 (1989).
- [23] E. Caurier, A.P. Zuker, A. Poves and G. Martínez-Pinedo, *Phys. Rev. C* **50** (1994) 225.
- [24] E.Caurier, J.L.Egido, G.Martinez-Pinedo, A.Poves, J.Retamosa, L.M.Robledo and A.P.Zuker, *Phys. Rev. Lett.* **75** (1995) 2466.
- [25] G. Martinez-Pinedo, A.P. Zuker, A. Poves and E. Caurier, *Phys. Rev. C* **55** (1997) 187.
- [26] A. Poves and A. Zuker, *Phys. Rep.* **70** (1981) 235.
- [27] E. Caurier, code ANTOINE, Strasbourg, 1989.
- [28] R.B.M. Mooy and P.W.M. Glaudemans, *Z. Phys.* **A312** (1983) 59.
- [29] A.P. Zuker, J. Retamosa, A. Poves and E. Caurier, *Phys. Rev. C* **52** (1995) R1741.
- [30] K. Eskola, *Phys. Lett.* **23** (1966) 471.
- [31] D. Seweryniak, I. Ahmad, H. Amro, D.J. Blumenthal, L.T. Brown, M.P. Carpenter, C.N. Davids, S. Fischer, D.J. Henderson, R.V.F. Janssens, T.L. Khoo, C.J. Lister, D. Nisius, T. Davinson, R.J. Irvine, P.J. Woods, W.B. Walters, I. Hibbert, C. Parry and R. Wadsworth, *Proceedings of the Conference on Nuclear Structure at the Limits, July 22-26 1996, ANL, Argonne* (1997) 247.
- [32] H. Mang, *Phys. Rev.* **119** (1960) 1069.
- [33] I. Perlman, F. Asaro, A. Ghiorso, A. Larsh and R. Lattimer, *Phys. Rev.* **127** (1962) 917.
- [34] P. Ring and P. Schuk, *The Nuclear Many Body Problem* (Springer-Verlag, New York, 1980).
- [35] A. Faessler, M. Ploszajczak and K.R.S. Devi, *Phys. Rev. Lett.* **36** (1976) 1028.

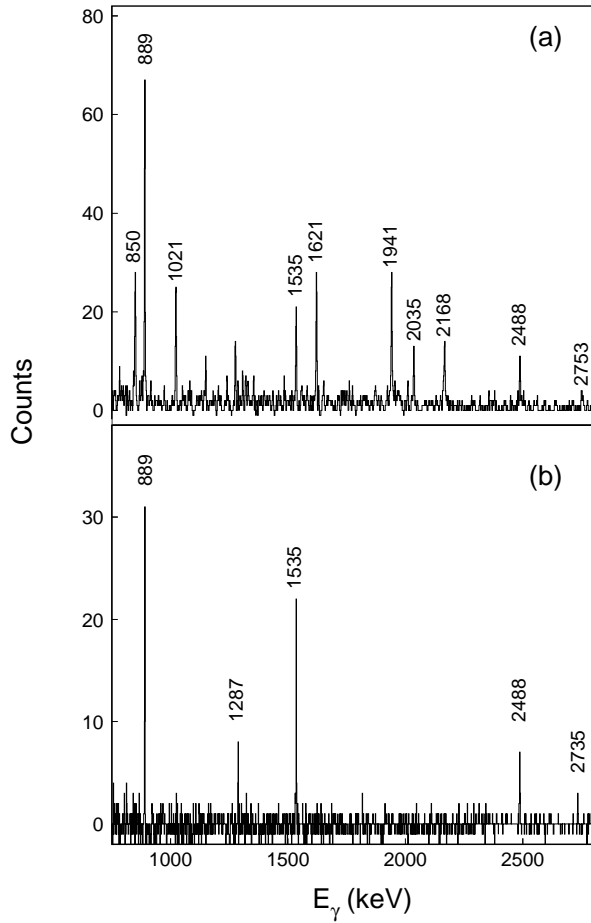


FIG. 1. Examples of double-gated spectra for some selected transitions assigned to ^{52}Fe : a) gates set on the first two yrast transitions, $2_1^+ \rightarrow 0_1^+$ and $4_1^+ \rightarrow 2_1^+$; the contaminant peaks between 1021 keV and 1535 keV belong to the strong channel ^{47}V ; b) gates set on the $2_1^+ \rightarrow 0_1^+$ and $8_2^+ \rightarrow 6_2^+$ transitions.

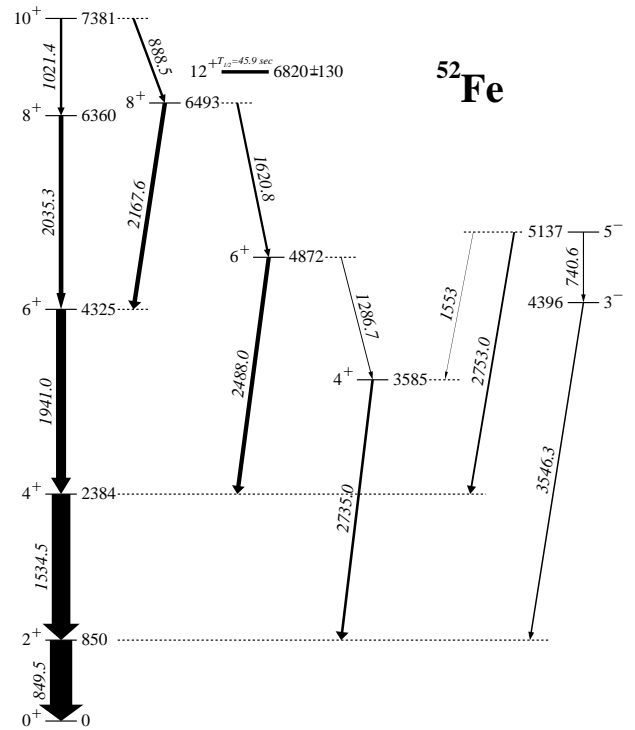


FIG. 2. Level scheme of ^{52}Fe , as obtained in the present experiment. The excitation energy of the 12^+ β^+ -decaying isomeric state is taken from ref. [11]

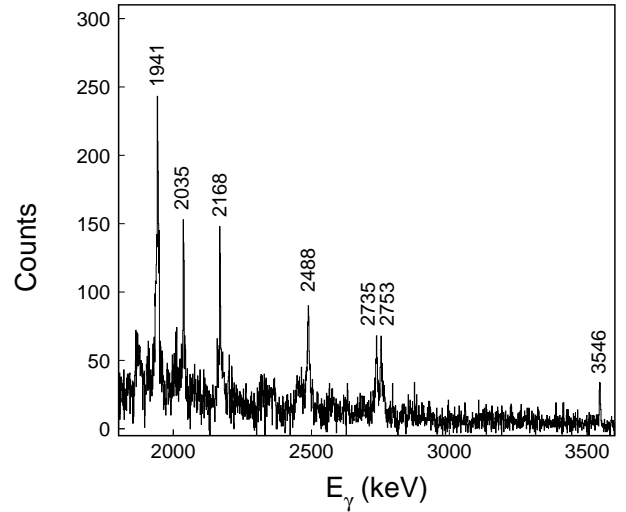


FIG. 3. High energy γ -ray spectrum at 90° in coincidence with the 850 keV transition.

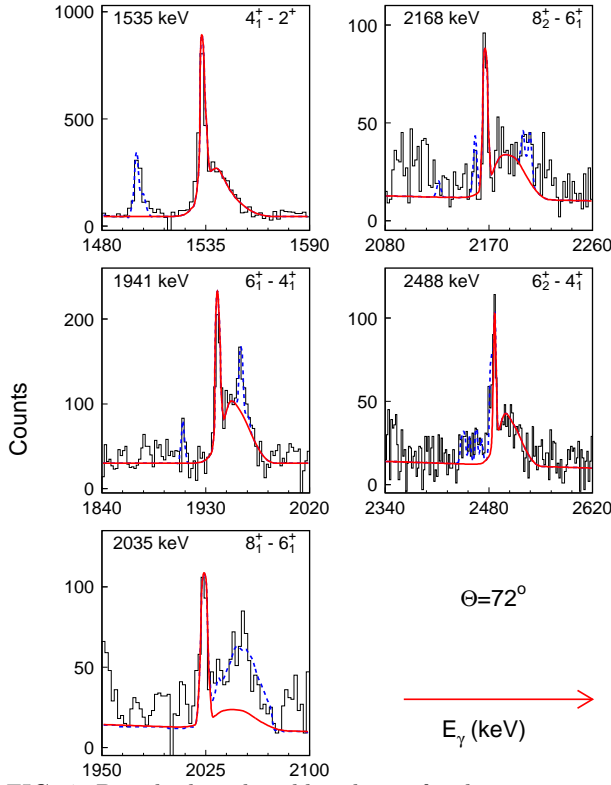


FIG. 4. Doppler broadened lineshapes for the transitions of 1535 keV ($4_1^+ \rightarrow 2^+$), 1941 keV ($6_1^+ \rightarrow 4_1^+$), 2035 keV ($8_1^+ \rightarrow 6_1^+$), 2168 keV ($8_2^+ \rightarrow 6_1^+$) and 2488 keV ($6_2^+ \rightarrow 4_1^+$), at 72 degrees. Full lines show least square fits performed with the LINE-SHAPE program and correspond to the mean lifetime values reported in Table II. The contaminant peaks are indicated by dashed lines.

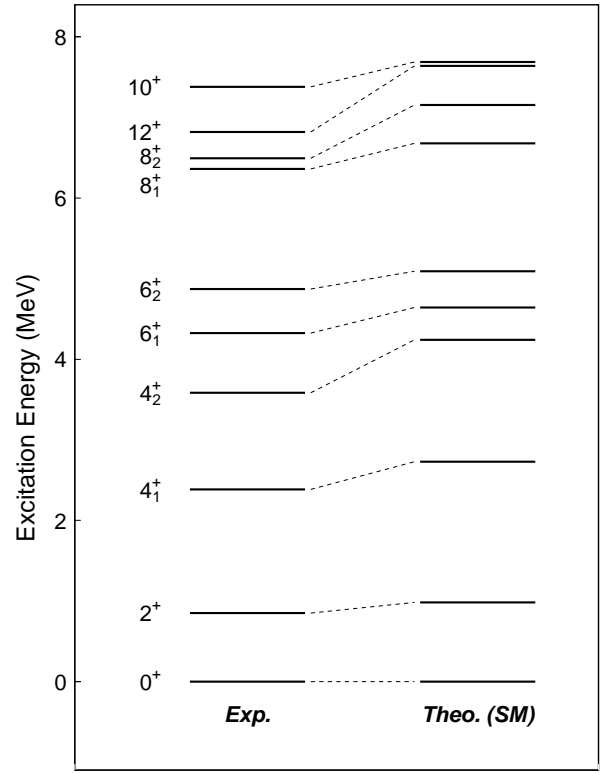


FIG. 5. Comparison between the experimental and the shell model positive parity energy levels in ^{52}Fe . Dashed lines connect levels of the same spin parity. The calculations reproduce the inversion between the 10^+ and 12^+ states.

TABLE I. Relative intensities, ADO ratios and spin assignments in ^{52}Fe .

E_γ (keV)	Intensity ^{a,b}	ADO ratios ^a	Assignment
740.6	5.5(6)	1.27(11)	$5^- \rightarrow 3^-$
849.5	-	-	$2^+ \rightarrow 0^+$
888.5	11.5(8)	1.20(8)	$10^+ \rightarrow 8_2^+$
1021.4	13.1(25)	-	$10^+ \rightarrow 8_1^+$
1286.7	5.0(10)	-	$6_2^+ \rightarrow 4_2^+$
1534.5	100.0(6)	1.16(4)	$4_1^+ \rightarrow 2^+$
1553	1.0(5)	-	$5^- \rightarrow 4_2^+$
1620.8	13.6(26)	-	$8_2^+ \rightarrow 6_2^+$
1941.0	55.0(30)	1.15(6)	$6_1^+ \rightarrow 4_1^+$
2035.3	21.0(30)	1.46(18)	$8_1^+ \rightarrow 6_1^+$
2167.6	20.7(20)	1.24(11)	$8_2^+ \rightarrow 6_1^+$
2488.0	21.9(15)	1.34(19)	$6_2^+ \rightarrow 4_1^+$
2735.0	15.0(17)	-	$4_2^+ \rightarrow 2^+$
2753.0	10.0(20)	-	$5^- \rightarrow 4_1^+$
3546.3	7.0(15)	0.92(8)	$3^- \rightarrow 2^+$

^aValues are extracted from spectra in coincidence with the 850 keV $2^+ \rightarrow 0^+$ transition.

^bErrors higher than 10% are specified.

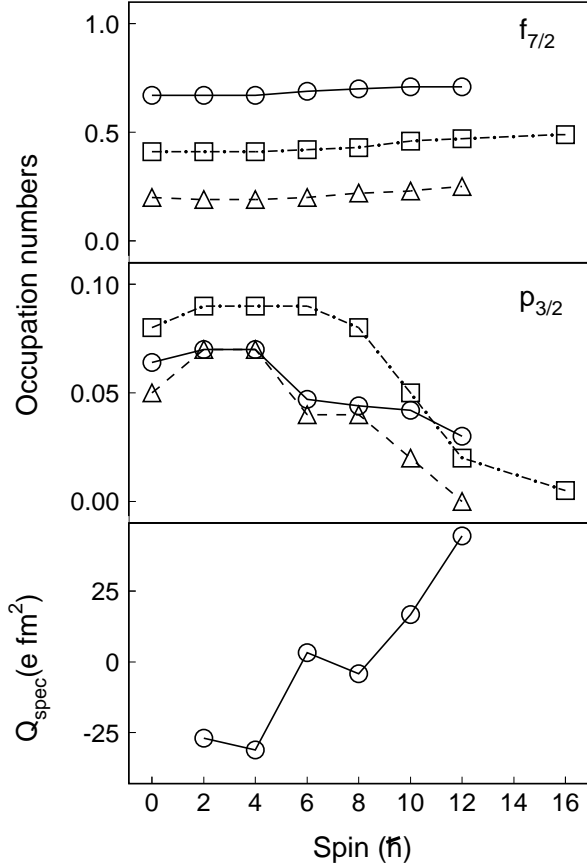


FIG. 6. The upper two panels show the occupation numbers of specific orbitals in the pf shell for the yrast even spin states in ^{44}Ti (triangles), ^{48}Cr (squares) and ^{52}Fe (circles) as extracted from the SM calculations. The lowest panel show the spectroscopic quadrupole moments of the yrast states in ^{52}Fe obtained with full fp spherical shell model calculations.

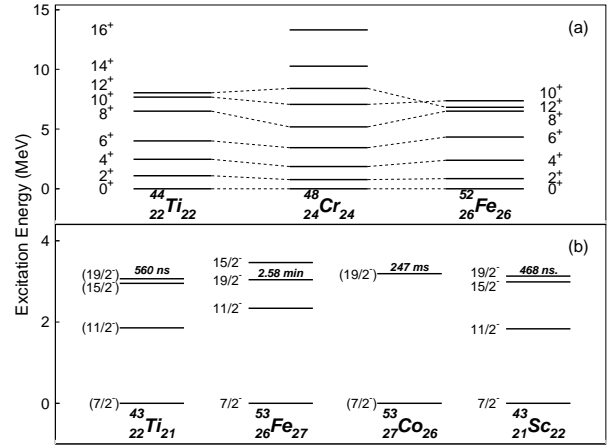


FIG. 7. Systematics of the yrast traps in the $f_{7/2}$ shell. a) Yrast states in the cross-conjugated nuclei ^{44}Ti and ^{52}Fe and in the self-conjugated nucleus ^{48}Cr showing the evolution of the collectivity along the $N=Z$ line in the $f_{7/2}$ shell. b) Other yrast traps showing the broken symmetry between cross conjugate nuclei.

TABLE II. Mean lifetimes of the states in ^{52}Fe as extracted from the present analysis compared with the ones of previous works and with the SM calculations. Statistical errors are specified for the side-feeding times.

E_x (keV)	E_γ (keV)	I_i	I_f	τ (ps)		τ_{SF} (ps)	$B(E2)$ ($e^2 fm^4$)	
				previous work [11]	present work		Exp.	SM
850	849.5	2	0	>1.0	-	-	<1844 ^a	154.5
2384	1534.5	4 ₁	2	0.40 ^{+0.29} _{-0.14}	0.32±0.08	0.06 ^{+0.03} _{-0.02}	300±69	223.5
4325	1941.0	6 ₁	4 ₁	-	0.24±0.08	0.04 ^{+0.02} _{-0.01}	124±40	117.9
4872	2488.0	6 ₂	4 ₁	-	0.30±0.12	0.04 ^{+0.03} _{-0.02}	29±14	83.3
6360	2035.3	8 ₁	6 ₁	-	0.21±0.08	0.01 ^{+0.01} _{-0.01}	74±25	85.6
6493	2167.6	8 ₂	6 ₁	-	0.26±0.06	0.01 ^{+0.01} _{-0.00}	43±15	11.3

^aValue calculated on the basis of the experimental limit given in ref. [11].